Is Spin Conserved in Heavy Metal Systems? Experimental and Theoretical Studies of the Reaction of Re^+ with Methane†

Matthew M. Armentrout,‡ Feng-Xia Li, and P. B. Armentrout*

Department of Chemistry, University of Utah, Salt Lake City, Utah 84112-0850

Received: March 27, 2004; In Final Form: June 29, 2004

A guided ion beam tandem mass spectrometer is used to study the reactions of atomic $^{187}Re^+$ with CH_4 and CD_4 and collision-induced dissociation (CID) of $ReCH_4^+$ with Xe. These studies examine the activation of methane by Re^+ in a low-pressure environment free of ligand supports or other reactive species. In the bimolecular reaction, $ReCH_2^+$ is efficiently produced in a slightly endothermic process and is the only ionic product observed at low energies, whereas at higher energies, ReH^+ dominates the product spectrum. Other products observed include ReC^+, $ReCH^+$, and $ReCH_3^+$. Modeling of these endothermic reactions yields 0 K bond dissociation energies in eV of $D_0(Re^+-C) = 5.12 \pm 0.04$, $D_0(Re^+-CH) = 5.84 \pm 0.06$, $D_0(Re^+-CH_2) = 4.14 \pm 0.06$, $D_0(Re^+-CH_3) = 2.22 \pm 0.13$. Analysis of the behavior of the cross sections suggests that formation of ReH^+, $ReCH_2^+$, and $ReCH_3^+$ occurs via an $H-Re^+-CH_3$ intermediate. CID of $ReCH_4^+$ reveals a bond energy of 0.53 ± 0.15 eV for Re^+-CH_4. The experimental bond energies compare favorably with theoretical calculations at the B3LYP/HW+/6-311++G(3df,3p) level with the exception of the singly bonded species (ReH^+, $ReCH_3^+$), where the Becke-half-and-half-LYP functional performs much better. Theoretical calculations also elucidate the reaction pathways for each product and provide their electronic structures. Overall we find that the dehydrogenation reaction, which occurs with an efficiency of $86 \pm 10\%$, must involve three facile spin changes ($2s + 1 = 7 \rightarrow 5 \rightarrow 3 \rightarrow 5$) indicating that little hint of spin conservation remains in this heavy-metal system.

Introduction

One of the interesting issues associated with the reactivity of transition metals is the influence of spin−orbit coupling. For third-row (5d block) metals, is spin even a useful concept or can it be ignored? One system for which such questions can potentially be answered quantitatively is the reactions of atomic metal ions with methane. Whereas none of the first- or second-row transition metal ions reacts with methane at thermal energies, Irikura and Beauchamp[1,2] found that several of the third-row transition metal ions (Ta^+, W^+, Os^+, Ir^+, and Pt^+) react exothermically to dehydrogenate methane, $M^+ + CH_4 \rightarrow MCH_2^+ + H_2$. This dramatic difference in reactivity between the first- and second-row transition metal ions and the third row is partially attributable to thermodynamic differences. The metal methylene bond energies are much stronger for the third-row metals, which can be related to the lanthanide contraction that alters the relative sizes of the valence s and d orbitals.[3] The lanthanide contraction is a consequence of 4f shielding and relativistic effects.

Not all the third-row metal ions react exothermically with methane, the exceptions being the early metals, La^+ (studied by Sunderlin and Armentrout)[4] and Hf^+,[1,2] along with Re^+ [1,2] and Au^+ (studied by Chowdhury and Wilkins).[5] The relative inactivity of the latter two metals can be attributed largely to the stable half-filled and filled 5d shell electron configurations, $6s^15d^5$ and $5d^{10}$, respectively. However, despite the stability of the $Re^+(^7S)$ state, this ion was observed to react with methane to form $ReCH_2^+$ when either translationally or electronically excited,[1] and the reverse reaction occurred at thermal energies. On this basis and the observation that Re^+ reacts with cyclopropane to form $ReCH_2^+$ at thermal energies, Irikura and Beauchamp assigned the Re^+-CH_2 bond energy as 4.4 ± 0.4 eV. Within these broad error limits, this agrees nicely with a calculated bond energy of 4.21 ± 0.17 eV by Irikura and Goddard.[6]

As part of an ongoing project to more fully elucidate the activation of H−H, H−C, and C−C bonds by third-row transition elements,[7] the present work uses guided ion beam mass spectrometry (GIBMS) to examine several reactions that are relevant to the activation of methane by Re^+. Numerous studies of the reactions of atomic transition metal ions (M^+) with hydrogen and small hydrocarbons have been conducted in the gas phase, where they are free from effects of solvent, stabilizing ligands, and metal supports.[8,9] These studies provide insight into the electronic requirements for the activation of C−C, C−H, and H−H bonds by transition metal ions in addition to establishing periodic trends for transition metals involved in these reactions. Among the methods used for such studies, GIBMS has the ability to determine accurate bond dissociation energies (BDEs) for $M^+-C_xH_y$ ($x = 0-3$, $y = 0 - 2x + 2$). This thermochemistry is of obvious interest and is relevant to the study of catalytic reactions involving transition-row elements.[10,11] Such gas-phase experiments are most complete for first- and second-row transition elements, although studies of third-row transition elements now include a number of experimental[1,2,4−7,12−18] and theoretical[1,3,6,12−14,19−24] studies.

Experimental Section

General Procedures. The guided ion beam mass spectrometer on which these experiments were performed has been described in detail previously.[25,26] Briefly, Re^+ ions are gener-

† Part of the special issue "Tomas Baer Festschrift".

‡ Summer Undergraduate Research Fellow, California Institute of Technology, Pasadena, CA.

10.1021/jp0486447 CCC: $27.50
Published on Web 08/07/2004

ated in a direct current discharge flow tube source described below, extracted from the source, accelerated, and focused into a magnetic sector momentum analyzer for mass analysis. Here, reactant ions containing the ^{187}Re isotope (62.6% natural abundance) are selected and then decelerated to a desired kinetic energy and focused into an octopole ion beam guide that uses radiofrequency electric fields to trap the ions in the radial direction and ensure complete collection of reactant and product ions.[27,28] The octopole passes through a static gas cell that contains the neutral collision/reaction partner at a low pressure (usually less than ~0.3 mTorr) so that multiple ion−molecule collisions are improbable. All products reported here result from single bimolecular encounters, as verified by pressure dependence studies. The unreacted parent and product ions are confined radially in the guide until they drift to the end of the octopole where they are extracted, focused, and passed through a quadrupole mass filter for mass analysis. Ions are subsequently detected with a secondary electron scintillation ion detector using standard pulse counting techniques. Reaction cross sections are calculated from product ion intensities relative to reactant ion intensities after correcting for background signals.[29] Uncertainties in absolute cross sections are estimated to be ±20%.

The kinetic energy of the ions is varied in the laboratory frame during the experiment by scanning the dc bias on the octopole rods with respect to the potential of the ion source region. Laboratory (lab) ion energies are converted to energies in the center-of-mass frame (CM) by using the formula $E_{CM} = E_{lab}\, m/(m + M)$, where m and M are the neutral and ionic reactant masses, respectively. Two effects broaden the cross section data: the kinetic energy distribution of the reactant ion and the thermal motion of the neutral reactant gas (Doppler broadening).[30] The absolute zero and the full width at half-maximum (fwhm) of the kinetic energy distribution of the reactant ions are determined using the octopole beam guide as a retarding potential analyzer, as described previously.[29] The distributions of ion kinetic energies, which are independent of energy, are nearly Gaussian and have a typical fwhm of 0.3−0.6 eV (lab) in these studies. Uncertainties in the absolute energy scale are ±0.05 eV (lab).

Ion Source. Re^+ ions are produced in a direct current discharge flow tube (DC/FT) source,[26] consisting of a cathode held at high negative voltage (0.7−1.5 kV) over which a flow of approximately 90% He and 10% Ar passes at a total pressure of 0.3−0.4 Torr and ambient temperature. In this work, the cathode is a rhenium cylinder attached to an iron holder. Ar^+ ions created in the discharge are accelerated toward the rhenium cathode, thereby sputtering Re^+. Re^+ ions are then swept down a 1 m long flow tube and undergo ~10^5 thermalizing collisions with He and ~10^4 collisions with Ar before entering the guided ion beam apparatus. Trace amounts of low-lying excited states of Re^+ are observed to survive these flow conditions, as found in preliminary reactions with CD_4 (Figure 1). Compared to the Langevin−Gioumousis−Stevenson (LGS) collision cross section,[31] this exothermic reactivity is about 1300 times smaller such that species comprising only 0.08% of the beam could account for this low-energy reactivity. These excited species are easily removed by introducing CH_4 to the flow tube about 15 cm downstream of the discharge zone at a pressure of ~100 mTorr (Figure 1). With the addition of such a cooling gas, the DC/FT source produces metal ions in the ground state. For example, on the basis of comparisons to a surface ionization source, the DC/FT source was found to generate Sc^+,[32] Fe^+,[33] Co^+,[34] Ni^+,[35] Ru^+,[36] Rh^+,[36] and Pd^+ [36] ions, with an average electronic temperature of 700 ± 400 K, and Y^+, Zr^+, Nb^+, and

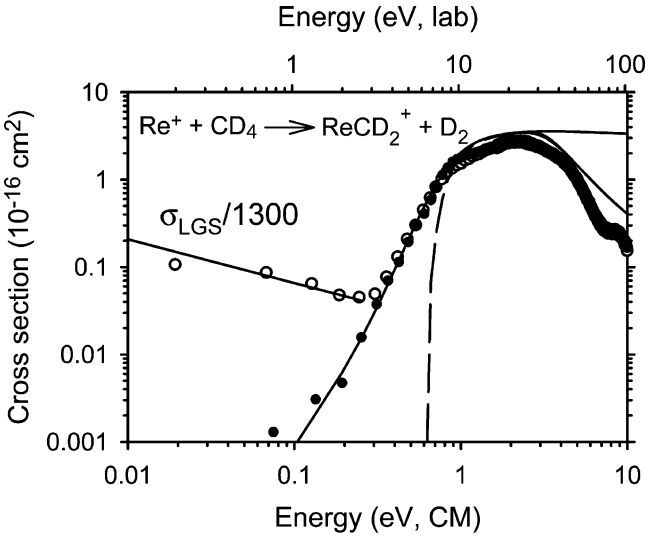

Figure 1. Cross sections for the dehydrogenation reaction of Re^+ with CD_4 as a function of kinetic energy in the center-of-mass frame (lower axis) and laboratory frame (upper axis). Results are shown for Re^+ produced without (open circles) and with (closed circles) methane added to the flow tube source. At low energy, the line shows the LGS collision cross section scaled down by a factor of 1300. At higher energies, the lines are the results of phase space calculations (see text) including (solid lines) and excluding (dashed line) the kinetic and internal energy distributions of the reactant neutral and ion.

Mo^+ ions with an average electronic temperature of 300 ± 100 K.[37] In the case of Re^+, even an elevated electronic temperature in this range (<1100 K) produces a pure beam of $^7S_3$ ground state because excited states are much too high in energy to be populated, i.e., the ^5D first excited state has an average energy of 1.827 eV with the ^5S second excited state at 2.135 eV.[38]

$ReCH_4^+$ is produced by the introduction of CH_4 into the flow tube about 15 cm downstream of the discharge zone at a pressure of ~2 mTorr. Three-body collisions with the He/Ar flow gas stabilize and thermalize the ions both rotationally and vibrationally. These ions are presumed to be in their ground electronic states, and the internal energy of these complexes should be well described by a Maxwell−Boltzmann distribution of rotational and vibrational states corresponding to 300 ± 100 K. Previous studies from this laboratory have shown that these assumptions are usually valid for molecular species.[39−43]

Data Analysis. The kinetic energy dependence of product cross sections is analyzed to determine E_0, the energy threshold for product formation at 0 K. E_0 differs from the apparent threshold observed under laboratory conditions because of the Maxwell−Boltzmann velocity distribution and internal energy of the neutral reactants and because of the kinetic and internal energy distributions of the reactant ions. Each of these contributions allows reactions to occur at energies below E_0. To determine E_0, endothermic reaction cross sections are modeled using eq 1,[44−46]

$$\sigma(E) = \sigma_0 \sum g_i (E + E_i - E_0)^n / E \qquad (1)$$

where σ_0 is an energy-independent scaling factor, E is the relative kinetic energy of the reactants, and n is an adjustable parameter. There is an explicit sum of the contributions from rovibrational states of the reactants at 300 K, denoted by i, having energies E_i and populations g_i, where $\Sigma g_i = 1$. The various sets of vibrational frequencies and rotational constants used to determine E_i in this work are taken from the literature

for CH_4 and CD_4 [47] and from ab initio calculations (see below) for $ReCH_4^+$. As noted above, the electronic energy of the Re^+ reactant is believed to be zero. Before comparison with the experimental data, eq 1 is convoluted with the kinetic energy distributions of the ions and neutral reactants at 300 K. The σ_0, n, and E_0 parameters are then optimized using a nonlinear least-squares analysis to give the best reproduction of the data.[45,46] Error limits for E_0 are calculated from the range of threshold values for different data sets over a range of acceptable n values combined with the absolute error in the energy scale.

Theoretical Calculation Section

All quantum chemistry calculations here are computed with the B3LYP hybrid density functional method[48,49] and performed with the Gaussian 98 suite of programs.[50] The B3LYP functional was used for most calculations done here because it provided reasonable results for the analogous $Pt^+ + CH_4$ system.[7] In all cases, the thermochemistry reported here is corrected for zero-point energy effects. Because several of the transition states of interest here involve bridging hydrogens, the rather large 6-311++G(3df,3p) basis set is used for carbon and hydrogen. This basis set gives good results for the thermochemistry of methane and dihydrogen, with deviations from experiment of less than 0.08 eV for the bond energies of $H-CH_3$ (4.406 vs 4.480 eV), H_2-CH_2 (4.666 vs 4.713 eV), H−CH (4.332 vs 4.360 eV), C−H (3.532 vs 3.465 eV), and H−H (4.505 vs 4.478 eV). (See Table 1 of ref 7 for thermochemistry used for all H, D, CH_x, and CD_x species.) For most calculations, the 60 core electrons of rhenium are described by the relativistic effective core potentials (ECP) of Hay−Wadt (HW),[51] with the valence electrons described by the Los Alamos double-ζ basis set (LANL2DZ). This basis set is optimized for neutral atoms, whereas the positive charge differentially contracts the s orbitals compared to the d orbitals. Hence, we used an altered valence basis set for Re as described by Ohanessian et al.,[3] which we designate as HW+.

The most appropriate choice for a level of theory has been thoroughly investigated for the first- and third-row transition metal methyl cations by Holthausen et al.[21] and for first-row transition metal methylene cations by Holthausen, Mohr, and Koch.[52] In the first study, these authors used B3LYP, Becke-half-and-half-LYP (BHLYP), and QCISD(T) methods with a basis set consisting of a polarized double-ζ basis on C and H and the Hay−Wadt relativistic ECP with valence electrons added. The symmetries of the metal methyl species were constrained to C_{3v}. For the first-row MCH_3^+ species (M = Sc−Cu), where experimental results are available for all metals,[9] these authors conclude that the B3LYP functional overbinds severely, with a mean average deviation (MAD) from experiment of 0.41 eV. The BHLYP functional and the QCISD(T) methods perform more accurately, with MADs of 0.18 and 0.20 eV, respectively. For the third-row elements, the bond energies calculated using B3LYP were again higher than those for BHLYP and QCISD(T). In contrast, for the metal methylene complexes,[52] the BHLYP functional predicts bond energies consistently below experimental values, whereas the performance of the B3LYP functional is quite good. In addition, these authors found that the results depended on the basis set used for the metal ion with an all electron basis providing better results than effective core potential (ECP) methods. On the basis of these results, the present study performed calculations for the various product ions using the BHLYP functional and the Stuttgart−Dresden (SD) ECP[53] for Re^+, along with QCISD(T) calculations using the HW+ ECP. Such calculations will be explicitly noted, but unless otherwise designated, our results will refer to the B3LYP/HW+/6-311++G(3df,3p) level of theory.

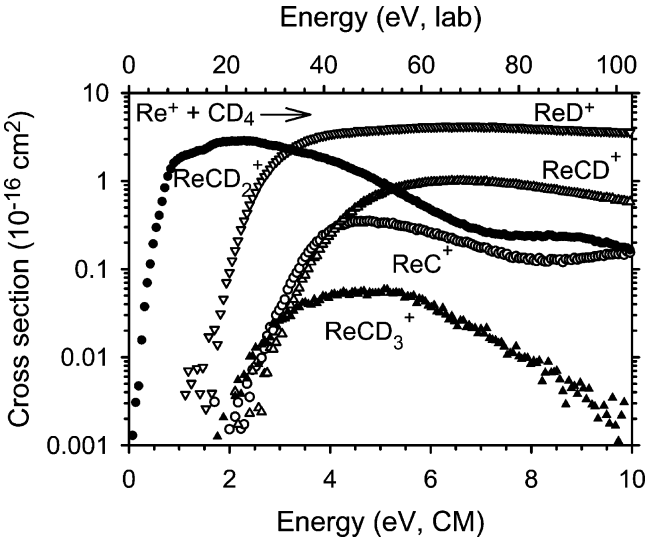

Figure 2. Cross sections for reaction of Re^+ (^7S) with CD_4 as a function of kinetic energy in the center-of-mass frame (lower axis) and laboratory frame (upper axis).

Using the HW+ basis set and B3LYP level of theory, we calculate a ^7S ground state for Re^+, with quintet states at 1.372 and 2.104 eV, a triplet state at 2.265 eV, and a singlet state at 5.583 eV. The excitation to the lowest lying quintet state was found to be 1.380, 1.493, and 1.484 eV for the B3LYP/SD, BHLYP/HW+, and BHLYP/SD combinations of functional/basis set, showing that the atomic excitations are not strongly dependent on the choices made, except that the QCISD(T) calculations find a splitting of 2.326 eV. In all cases, the first quintet state exhibits spin contamination ($s^2 = 6.95$ rather than 6.0) and clearly contains some $6s^15d^5$ character, whereas the second value appears to be pure $5d^6$ (^5D) ($s^2 = 6.0$). These septet−quintet excitation energies can be favorably compared with the experimental excitation energies of 1.827 for the ^5D first excited state and 2.135 for the ^5S second excited state.[38] Excitation energies for triplet and singlet states of Re^+ have not been experimentally identified largely because of the extensive spin−orbit coupling for this heavy metal. The difficulties associated with accurate calculations of the various spin states of a heavy metal like Re^+ are illustrated by excitation energies given in the literature. Ohanessian et al. calculate a ^7S ground state with a $^5D(5d^6)$ state at 2.64 eV and a $^5D(6s^25d^4)$ state at 2.94 eV.[3] Dai and Balasubramanian calculated an excited $^5G(5d^6)$ state lying at 2.687 eV, with a triplet and singlet at 4.182 and 4.377 eV, respectively.[54] Oddly, the calculations of Holthausen et al.[21] find a ground state of $^5D(5d^6)$ using the B3LYP and BHLYP functionals, with the ^7S state lying 0.26 and 0.10 eV higher in energy, respectively. QCISD and QCISD(T) methods provide the correct ordering with quintet excitation energies of 1.11 and 1.09 eV, respectively. As can be seen, not only is there no consensus among these theoretical studies but none of the calculations does a particularly good job of quantitatively predicting the experimental excitation energies.

Experimental Results

Reaction of Re^+ with Methane. Figure 2 shows cross sections for the reaction of CD_4 with Re^+ quenched in the flow

tube source with CH_4, which yields product ions as shown in reactions 2−6:

$$Re^+ + CD_4 \rightarrow ReD^+ + CD_3 \quad (2)$$

$$\rightarrow ReC^+ + 2D_2 \quad (3)$$

$$\rightarrow ReCD^+ + D_2 + D \quad (4)$$

$$\rightarrow ReCD_2^+ + D_2 \quad (5)$$

$$\rightarrow ReCD_3^+ + D \quad (6)$$

Analogues of these reactions were examined for Re^+ and CH_4 and yielded results consistent with those shown in Figure 2. Only results for the perdeuterated species are shown here because use of CD_4 reduces mass overlap and allows for a more accurate measurement of product intensities over a greater energy range.

As can be seen from Figure 2, once the Re^+ ions are properly quenched, all reactions with methane are endothermic. This is consistent with the previous ICR studies[1,2] in which no exothermic reactions were noted but translationally or electronically excited ions did react to form $ReCH_2^+$. At energies greater than 2 eV, the $ReCD_2^+$ cross section begins to decline. This decline corresponds well with the apparent thresholds of the other products observed; however, only the cross section of ReD^+ is large enough to account for the initial drop in intensity of $ReCD_2^+$. From this, we can infer that either there is a decomposition reaction of $ReCD_2^+ \rightarrow ReD^+ + CD$ or that the formation of $ReD^+ + CD_3$ is competitive with the formation of $ReCD_2^+ + D_2$. However, decomposition of $ReCD_2^+$ to $ReD^+ + CD$ cannot occur until much higher energies such that formation of ReD^+ and $ReCD_2^+$ must be competitive with each another. Such competition can most easily be explained if these two products share a common intermediate, as discussed below.

Formations of $ReCD_3^+$ and ReD^+ arise from similar apparent thresholds near 1.5 eV, which implies that the single bonds of Re^+-D and Re^+-CD_3 are comparable in strength. Despite the similar energetics, ReD^+ dominates the product spectrum at high energies. This is partly a result of angular momentum effects,[4,55−57] as discussed below.

$ReCD^+$ and ReC^+ are formed by elimination of molecular deuterium from $ReCD_3^+$ and $ReCD_2^+$, respectively. This decomposition pathway is another primary reason for the small cross section of $ReCD_3^+$ because dehydrogenation requires little energy (see below). It is also possible that $ReCD_2^+$ could lose a D atom to form $ReCD^+$. Other possible reaction pathways for forming ReC^+ that stem from either $ReCD_3^+$ or $ReCD^+$ require much higher energies than the dehydrogenation of $ReCD_2^+$.

The cross sections of $ReCD_2^+$ and ReC^+ are observed to increase slightly at about 7 and 8.5 eV, respectively. The second feature in the $ReCD_2^+$ cross section must be attributed to formation of $ReCD_2^+ + 2D$ and must occur by loss of a D atom from $ReCD_3^+$. The second feature in the ReC^+ cross section results from dehydrogenation of the $ReCD_2^+$ ions formed by this second pathway.

$ReCH_4^+ + Xe$. To characterize the $ReCH_4^+$ species involved as an intermediate in the reaction of Re^+ with CH_4, collision-induced dissociation (CID) of $ReCH_4^+$ with Xe gas was performed to determine the bond dissociation energy (BDE) of Re^+-CH_4. Reactions 7−9 were the only processes observed, as shown in Figure 3.

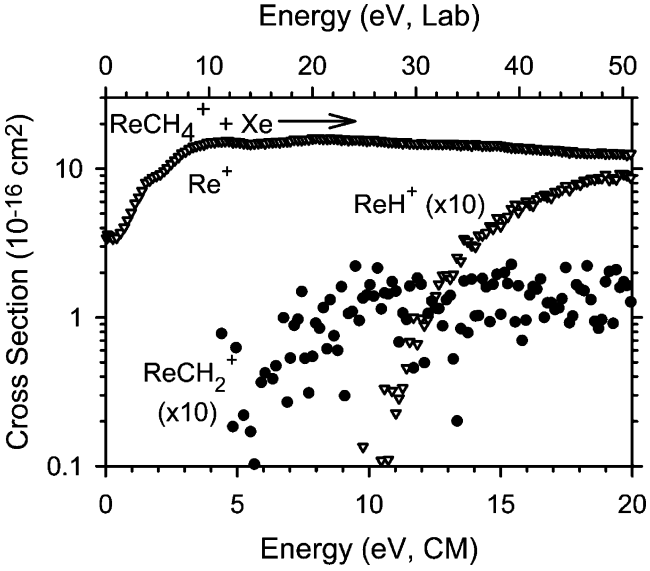

Figure 3. Cross sections for collision-induced dissociation of $ReCH_4^+$ with Xe as a function of kinetic energy in the center-of-mass frame (lower axis) and laboratory frame (upper axis).

$$ReCH_4^+ + Xe \rightarrow Re^+ + CH_4 + Xe \quad (7)$$

$$\rightarrow ReH^+ + CH_3 + Xe \quad (8)$$

$$\rightarrow ReCH_2^+ + H_2 + Xe \quad (9)$$

The dominant process is the simple cleavage of Re^+ from CH_4 with a very low-energy threshold. At higher energies, small amounts of ReH^+ and $ReCH_2^+$ are formed. The ReH^+ cross section has a very clean threshold near 10 eV. The $ReCH_2^+$ cross section is quite noisy because of overlap with the much more intense $ReCH_4^+$ reactant ion signal but appears to have a threshold near 5 eV.

Thermochemical and Theoretical Results

The cross sections from each experiment are analyzed using eq 1, as explained above. The optimal values of the parameters in eq 1 are listed in Table 1 for each product cross section. Because the rotational, translational, and vibrational energy distributions are included explicitly in the modeling, all E_0 thresholds determined by eq 1 correspond to 0 K values. From the measured thresholds, the BDEs of the rhenium−ligand cations are calculated using

$$D_0(Re^+-L) = D_0(R-L) - E_0 \quad (10)$$

where the $D_0(R-L)$ values can be calculated using the heats of formation summarized previously.[7] This equation assumes that there are no activation barriers in excess of the endothermicity of a given reaction, an assumption that is often true for ion−molecule reactions because of the long-range attractive forces.[29,46] Table 2 provides a summary of the BDEs derived and comparison with literature values, as discussed below. Tables 3 and 4 provide summaries of the B3LYP theoretical results (energies and structures) for each of the product ions and their excited states. These results are discussed in detail in the following sections for each species.

Re^+-H. The bond energy of ReH^+ has recently been measured from the reaction of Re^+ with H_2 and D_2, yielding a value of 2.29 ± 0.07 eV.[58] From eq 10, $D_0(D-CD_3) = 4.58$

TABLE 1: Parameters of Eq 1 Used in Modeling the Reaction Cross Sections

reaction		σ_0	n	E_0 (eV)	$D_0(Re^+-L)$ (eV)
$Re^+ + CD_4$	$\rightarrow ReD^+ + CD_3$	9.2 ± 1.0	0.8 ± 0.1	2.48 ± 0.04	2.10 ± 0.04
	$\rightarrow ReCD_3^+ + D$	0.13 ± 0.01	0.8 ± 0.1	2.52 ± 0.11	2.06 ± 0.11
	$\rightarrow ReCD_2^+ + D_2$	3.8 ± 0.3	1.0 ± 0.1	0.58 ± 0.06	4.24 ± 0.06
	$\rightarrow ReCD^+ + D_2 + D$	1.7 ± 0.5	1.3 ± 0.2	3.49 ± 0.14	5.76 ± 0.14
	$\rightarrow ReC^+ + 2\ D_2$	1.0 ± 0.2	1.1 ± 0.1	3.12 ± 0.03	5.08 ± 0.03
$Re^+ + CH_4$	$\rightarrow ReH^+ + CH_3$	7.0 ± 1.2	0.9 ± 0.1	2.38 ± 0.04	2.10 ± 0.04
	$\rightarrow ReCH_3^+ + H$	0.11 ± 0.01	0.8 ± 0.1	2.49 ± 0.06	1.99 ± 0.06
	$\rightarrow ReCH_2^+ + H_2$	4.3 ± 0.1	0.9 ± 0.1	0.61 ± 0.03	4.10 ± 0.03
	$\rightarrow ReCH^+ + H_2 + H$	1.7 ± 0.3	1.0 ± 0.1	3.23 ± 0.03	5.84 ± 0.03
	$\rightarrow ReC^+ + 2\ H_2$	0.36 ± 0.09	1.4 ± 0.1	2.90 ± 0.03	5.16 ± 0.03
$ReCH_4^+ + Xe$	$\rightarrow Re^+ + CH_4$	6.8 ± 1.0	1.6 ± 0.1	0.53 ± 0.15	0.53 ± 0.15
	$\rightarrow ReH^+ + CH_3$	0.8 ± 0.2	1.4 ± 0.1	10.8 ± 0.6	

TABLE 2: Comparison of Experimental and Theoretical Thermochemistry for ReH^+ and $ReCH_y^+$ ($y = 0-4$) Species

	this work							
		theory[a]						
		B3LYP		BHLYP		QCISD(T)	previous work	
species	exp	HW+	SD	HW+	SD	HW+	exp	theory
Re^+-H ($^6\Sigma^+$)	2.29 ± 0.07[b]	2.62	2.54	2.38	2.32	2.24		1.93[c]
Re^+-CH_3 ($^6A_1$)	2.22 ± 0.13	2.66	2.58	2.26	2.19	2.50		2.63 ± 0.22[d]
								2.54 ± 0.22[d]
Re^+-CH_2 ($^5B_1$)	4.14 ± 0.06	4.30	4.18	3.61	3.53	3.93	4.4 ± 0.4[e]	4.21 ± 0.17[f]
Re^+-CH ($^4\Sigma^-$)	5.84 ± 0.06	5.87	5.71	4.87	4.75	5.67		5.1[g]
Re^+-C ($^3\Sigma^-$)	5.12 ± 0.04	4.78	4.69	3.68	3.63	4.48		
Re^+-CH_4 ($^7A_1$)	0.53 ± 0.15	0.33	0.26	0.28	0.22	0.37		
$HReCH_3^+$ ($^5A'$)		0.87	0.75	0.33	0.24	0.50		
$(H)_2ReCH_2^+$ (^3A)		0.57	0.40	−0.47	−0.61	0.17		

[a] Calculations using the level of theory indicated with a 6-311++G(3df,3p) basis set on C and H and the ECP indicated on Re^+. HW+ = Hay−Wadt (ref 51) as adjusted for the cation by Ohanessian et al. (ref 3). SD = Stuttgart−Dresden (ref 53). [b] Reference 58. [c] Reference 3. [d] Reference 21. [e] Reference 2. [f] Reference 6. [g] Estimated in ref 6.

eV, and a calculated zero-point energy difference between ReD^+ and ReH^+ of 0.037 eV, this predicts that the threshold for formation of ReD^+ in reaction 2 should be 2.25 ± 0.07 eV. Our analysis of this cross section (Table 1) measures a higher threshold of 2.48 ± 0.04 eV. This value is higher than the apparent threshold in Figure 2 by a significant amount because of the kinetic energy distributions of the reactants. Similarly, the predicted value of E_0 for Re^+-H obtained in the methane system is 2.19 ± 0.07 eV, whereas the measured threshold is 2.38 ± 0.04 eV. Thus, the CH_4 and CD_4 systems are behaving similarly to each another but do not agree with the thermodynamic results obtained from the H_2 and D_2 systems. On average, the thresholds in the methane systems are higher in energy by 0.21 ± 0.08 eV, a discrepancy that can be attributed to a competitive shift. Whereas there are no competing channels in the reactions of Re^+ with H_2 and D_2, the dehydrogenation reaction 5 strongly competes with reaction 2 at its threshold. This competition can delay the apparent onset for formation of ReD^+ (ReH^+) in the methane systems. The complexity of this reaction system prevents quantitative analyses of these data that include this competition, but simple phase space calculations (see below) confirm that such a competitive shift can occur in the methane reactions with a magnitude comparable to that observed experimentally.

The 2.29 ± 0.07 eV value for $D_0(Re^+-H)$ is somewhat higher than the results of theoretical calculations by Ohanessian et al.[3] of 1.93 eV, the only previous work on this BDE. The present calculations find a BDE for Re^+-H of 2.62 eV when using the B3LYP functional and HW+ ECP. A slightly lower value of 2.54 eV was obtained when using the SD ECP on Re. As noted above, Holthausen et al.[21] have previously characterized the overbinding of the B3LYP functional for the comparable third-row transition metal ion methyl cations, which also involve a single covalent metal−ligand bond. These authors suggested the BHLYP functional as a useful alternative, and indeed, we obtain lower bond energies of 2.38 (HW+) and 2.32 (SD) eV, in good agreement with the experimental results. For the metal methyl cations, these authors applied an empirical correction of −0.22 eV to their BHLYP bond energies, but such a correction should be basis set dependent, making it inappropriate here. Some verification that the BHLYP is performing better here is the finding that a bond energy of 2.24 eV is calculated at the QCISD(T) level.

The ground state for ReH^+ is a $^6\Sigma^+$ resulting from a covalent bond between a 6s5d hybrid orbital on Re^+ and the H(1s) orbital.[3] In this molecule, the nonbonding metal valence orbitals, all singly occupied, are $\pi^2\delta^2\sigma^1$, where the σ orbital is the other sd hybrid. The bond length determined here, 1.647 Å, is similar to that calculated by Ohanessian et al., 1.659 Å. We also determined excitation energies for a number of excited states, as described in detail elsewhere.[58]

Re^+-CH_3. The BDE of Re^+-CD_3 derived from the CD_4 system is 2.06 ± 0.11 eV and the BDE of Re^+-CH_3 from the methane system is 1.99 ± 0.06 eV. After correcting for the zero-point energy differences in these two values (0.028 eV), we obtain a weighted average value of 2.01 ± 0.10 eV for the BDE of Re^+-CH_3. This value is similar to the BDE for Re^+-H obtained from a routine analysis of the ReH^+ and ReD^+ channels, as expected given that a single covalent bond to Re^+ is formed in each molecule. As noted above, the ReH^+ BDE derived in this way is too small because of competition with the dehydrogenation reaction. If we presume that the $ReH^+ + CH_3$ and $ReCH_3^+ + H$ channels are similarly affected by this competition, then the shift determined for ReH^+ (0.21 ± 0.08 eV) can be used here to provide our best estimate of the $ReCH_3^+$ bond energy as 2.22 ± 0.13 eV.

A thorough theoretical investigation of the first- and third-row transition metal methyl cations has been conducted by

TABLE 3: Theoretical Energies of Reactants and Products Calculated at the B3LYP/HW+/6-311++G(3df,3p) Level of Theory

compd	state	energy (h)	zero point energy (h)	E_{rel} (eV)[a]
H	^2S	−0.502 257		
H_2	$^1\Sigma_g^+$	−1.180 030	0.010 064	
C	^3P	−37.857 442		
CH	$^2\Pi$	−38.495 898	0.006 450	0.000
	$^4\Sigma$	−38.462 172	0.006 943	0.931
CH_2	$^3B_1$	−39.167 949	0.017 169	
CH_3	$^2A''$	−39.857 664	0.029 685	
CH_4	$^1A_1$	−40.536 527	0.044 525	
Re^+	^7S	−78.672 789		0.000
	^5X	−78.622 374		1.372
	^5D	−78.595 458		2.104
	^3X	−78.589 546		2.265
	^1X	−78.467 609		5.583
ReH^+	$^6\Sigma^+$	−79.276 184	0.004 763	0.000
ReC^+	$^3\Sigma^-$	−116.708 532	0.002 474	0.000
	$^5\Sigma^-$	−116.682 233	0.002 405	0.714
	$^5\Pi$	−116.658 012	0.001 888	1.359
	$^3\Delta$	−116.629 533	0.002 510	2.151
	$^3\Pi$	−116.553 563	0.001 866	4.200
	$^1\Sigma$	−116.448 128	0.002 344	7.082
$ReCH^+$	$^4\Sigma^-$	−117.391 147	0.013 172	0.000
	$^2\Delta$	−117.328 500	0.013 038	1.701
	$^6A''$	−117.294 925	0.010 212	2.538
	$^2\Pi/\Phi$	−117.269 923	0.012 666	3.285
	$^6\Sigma/A'$	−117.264 931	0.010 838	3.371
	$^4A'$	−117.221 666	0.008 213	4.477
$ReCH_2^+$	$^5B_1$	−118.003 802	0.022 186	0.000
	$^3B_1$	−117.970 162	0.022 251	0.917
	$^7A'$	−117.938 019	0.020 977	1.757
	$^3B_2$	−117.934 093	0.022 525	1.906
	$^3A_2$	−117.926 811	0.023 619	2.134
	$^3A_1$	−117.915 278	0.023 231	2.437
	$^5A_1$	−117.887 881	0.020 690	3.114
	$^7A_1$	−117.885 566	0.021 543	3.200
$ReCH_3^+$	$^6A_1$	−118.632 705	0.034 281	0.000
	$^4A'$	−118.589 923	0.033 915	1.154
	$^4A''$	−118.568 324	0.032 929	1.715
	^2E	−118.568 145	0.033 797	1.744

[a] Energy relative to the ground-state species for each compound including zero-point energies (unscaled).

Holthausen et al.,[21] who used B3LYP, BHLYP, and QCISD(T) levels of theory. These three methods gave predicted Re^+-CH_3 bond energies of 3.36, 2.85, and 2.38 eV, respectively. On the basis of results for first-row metal methyl cations compared to experiment, empirical corrections of −0.22 and +0.16 eV for the BHLYP and QCISD(T) methods were applied leading to final suggested bond energies of 2.63 and 2.54 eV with estimated errors of ±0.22 eV. These values are somewhat above our adjusted experimental value of 2.22 eV and well above the uncorrected value (2.01 eV), suggesting that the former is more likely to be correct.

For our theoretical calculations, we obtain a value for $D_0(Re^+-CH_3)$ of 2.66 eV, in good agreement with the final predictions of Holthausen et al.[21] Use of the SD ECP lowers our predicted bond energy by only 0.08 eV; however, the BHLYP functional drops the calculated bond energies to 2.26 (HW+) and 2.19 (SD) eV, and the QCISD(T) calculations yield 2.50 eV (Table 2). The BHLYP values are in good agreement with experiment, as also noted for the ReH^+ species. Note that the bond energies for ReH^+ and $ReCH_3^+$ in both the experimental and theoretical results are similar, consistent with both having comparable single covalent metal−ligand bonds. Thus, whatever the origin of any discrepancy between experiment and any particular level of theory, the same discrepancy is occurring for both ReH^+ and $ReCH_3^+$, as assumed in deriving our adjusted value for the BDE of the latter.

The ground state of $ReCH_3^+$ was found to be $^6A_1$ with C_{3v} symmetry. The Re−C and C−H bond lengths, and ReCH bond angles calculated here (2.061 Å, 1.093 Å, and 108.5°) are comparable to those calculated by Holthausen et al. (2.042 Å, 1.100 Å, and 108.6°, B3LYP; 2.068 Å, 1.096 Å, and 109.0°, QCISD(T)).[21] We find an excited quartet state lying 1.15 eV higher in energy (Table 3), which has no symmetry although it is essentially a $^4A'$ state. A $^4A''$ state lies 1.72 eV above the ground state, and a ^2E state (C_{3v} symmetry) was found at 1.74 eV. The $^4A''$ state is the only state that shows some Re−H bonding character, as shown by the short Re−H bond distance and acute ReCH bond angle (Table 4).

Re^+-CH_2. The thresholds for dehydrogenation, reaction 5, and its perprotiated analogue, are 0.58 ± 0.06 eV for the CD_4 system and 0.61 ± 0.03 eV for the CH_4 system. These thresholds correspond to BDEs for Re^+-CD_2 of 4.19 ± 0.06 eV and for Re^+-CH_2 of 4.10 ± 0.03 eV. After correction of the former value for the zero-point energy difference of 0.023 eV, the weighted average of these values yields $D_0(Re^+-CH_2) = 4.14 \pm 0.06$ eV, where the uncertainty is 2 standard deviations of the mean. This is consistent with earlier results of Irikura and Beauchamp[2] who determined a Re^+-CH_2 BDE of 4.4 ± 0.4 eV using ICR mass spectrometry. This value was derived as the mean of the 298 K bond energies of cyclopropane, which reacts with Re^+ exothermically to form $ReCH_2^+$, and methane, where the reaction is endothermic, as verified here.

Irikura and Goddard previously calculated that $ReCH_2^+$ has a $^5B_1$ ground state with a calculated D_e of 3.69 eV.[6] These authors also included an empirical correction of 0.52 ± 0.22 eV, leading to their final recommended 0 K bond energy of 4.21 ± 0.17 eV, in good agreement with our experimental result. Excited states, $^7B_1$ and $^3B_1$, were found lying 0.60 and 1.90 eV higher in energy, respectively. The present calculations (B3LYP/HW+) also find a $^5B_1$ ground state with a bond energy of 4.30 eV, in good agreement with the previous recommended theoretical value and in reasonable agreement with experiment. Use of the SD-ECP leads to a bond energy of 4.18 eV, whereas shifting to the BHLYP functional provides bond energies well below experiment, 3.61 (HW+) and 3.53 (SD) eV, as previously observed by Holthausen et al.[52] The QCISD(T) methodology yields an intermediate value of 3.93 eV. Our ground-state geometry of $r(Re-C) = 1.861$ Å, $r(C-H) = 1.092$ Å, and $\angle ReCH = 122.0°$ is comparable to that calculated by Irikura and Goddard, $r(Re-C) = 1.908$ Å, $r(C-H) = 1.083$ Å, and $\angle ReCH = 122.0°$. We also found a $^3B_1$ state lying 0.92 eV higher in energy and a $^7A'$ state lying 1.76 eV above the ground state. This latter state is nonplanar (dihedral angle of 156°) with an umbrella motion that leads to a planar $^7B_1$ transition state lying only 0.006 eV higher in energy (calling into question whether the nonplanar structure is an artifact of the level of theory). Calculations also located stable (no imaginary frequencies) excited states of $^5A_1$, $^3A_1$, $^3A_2$, $^3B_2$, and $^7A_1$ lying 3.11, 2.44, 2.13, 1.91, and 3.20 eV, respectively, higher than the $^5B_1$ state (Table 3).

Re^+-CH. Cross sections from the perdeuterated methane and perprotio methane experiments yield thresholds of 3.49 ± 0.14 and 3.23 ± 0.03 eV for formation of $ReCD^+$ and $ReCH^+$, respectively. These thresholds correspond to BDEs of 5.76 ± 0.14 and 5.84 ± 0.03 eV (Table 1). The calculated zero-point energy difference between these two species is 0.026 eV such that the weighted mean of these values is 5.84 ± 0.06 eV, where the uncertainty is 2 standard deviations of the mean. We do

TABLE 4: Theoretical Structures of Reactants and Products Calculated at the B3LYP/HW+/6-311++G(3df,3p) Level of Theory[a]

compd	state	r(Re−H)	r(Re−C)	r(C−H)	∠ReCH	∠HCH	dihedral angle
H_2	$^1\Sigma_g^+$						
CH	$^2\Pi$			1.122			
	$^4\Sigma$			1.093			
CH_2	$^3B_1$			1.078		135.1	
CH_3	$^2A''$			1.078 (3)		120.0 (3)	
CH_4	$^1A_1$			1.088 (4)		109.5 (6)	
ReH^+	$^6\Sigma^+$	1.647					
ReC^+	$^3\Sigma^-$		1.665				
	$^5\Sigma^-$		1.716				
	$^5\Pi$		1.813				
	$^3\Delta$		1.693				
	$^3\Pi$		1.773				
	$^1\Sigma$		1.728				
$ReCH^+$	$^4\Sigma^-$		1.706	1.086	180.0		
	$^2\Delta$		1.700	1.085	180.0		
	$^6A''$		1.900	1.096	135.7		
	$^2\Pi/\Phi$		1.787	1.088	180.0		
	$^6\Sigma/A'$		1.893	1.083	180.0		
	$^4A'$		2.680	1.106	170.6		
$ReCH_2^+$	$^5B_1$		1.861	1.092 (2)	122.0 (2)	116.0	180.0
	$^3B_1$		1.842	1.094 (2)	122.1 (2)	115.8	180.0
	$^7A'$		2.094	1.087 (2)	118.2 (2)	119.1	155.9
	$^3B_2$		1.844	1.094 (2)	121.7 (2)	116.7	180.0
	$^3A_2$		1.872	1.095 (2)	123.2 (2)	113.7	180.0
	$^3A_1$		1.873	1.095 (2)	123.2 (2)	113.5	180.0
	$^5A_1$		1.932	1.089 (2)	120.3 (2)	119.4	180.0
	$^7A_1$		2.327	1.096 (2)	125.6 (2)	108.8	180.0
$ReCH_3^+$	$^6A_1$		2.061	1.093 (3)	108.5 (3)	110.4 (3)	±120.0
	$^4A'$		2.039	1.094	108.8 (2)	109.3	±120.5
				1.096 (2)	109.1	110.4 (2)	
	$^4A''$	1.897	2.039	1.094	69.9	108.3 (2)	±99.7
				1.096 (2)	121.3 (2)	114.7	
	^2E		2.028	1.096 (3)	108.6 (3)	110.3 (3)	±120.0

[a] Bond lengths are in Å. Bond angles are in degrees. Degeneracies are listed in parentheses.

not believe that competition with other channels is an important factor for this process because it is a subsequent step, i.e., decomposition of one of the primary ions (see below). However, because of this possibility, the bond energy is most conservatively viewed as a lower limit to the true thermodynamic value.

This value is greater than the estimate of Irikura and Goddard, 5.1 eV, derived by estimating an intrinsic bond strength and correction for promotion and exchange energies.[6] However, it is in reasonable agreement with the bond energies calculated here of 5.87 (HW+) and 5.71 (SD) eV. As for the rhenium methylene cation, values calculated using the BHLYP functional are well below experiment, 4.87 (HW+) and 4.75 (SD) eV (Table 2), whereas the QCISD(T) value of 5.67 eV is much closer to the B3LYP values and experiment.

Our calculations indicate that the ground state of $ReCH^+$ is $^4\Sigma^-$, in which a Re≡C triple bond is formed. The valence orbital occupation is $\sigma^2\pi^4\delta^2\sigma^1$, where the first σ orbital is a bonding combination of the $2p_z$(C) and $5d_{z^2}$(Re) orbitals, the upper σ orbital is a $6s5d_{z^2}$ hybrid (largely a torus surrounding the bonding axis), the π orbitals are the expected $2p_{x,y}$(C)−$5d_{xz,yz}$(Re) bonding molecular orbitals, the δ are pure metal $5d_{xy,x^2-y^2}$(Re) orbitals. The lowest lying excited state is $^2\Delta$ lying 1.70 eV higher in energy and has a $\sigma^2\pi^4\delta^3\sigma^0$ configuration. The lowest lying state having sextet spin is the $^6A''$ state, lying 2.54 eV above the $^4\Sigma^-$, with a $\sigma^2\pi^3\delta^2\sigma^1\pi^{*1}$ configuration. Here, the $\pi-\pi^*$ excitation needed to give the high-spin forces the geometry to be bent, ∠ReCH = 136° (Table 4). Other stable (no imaginary frequencies) excited states were also found: $^2\Pi/\Phi$ (3.28 eV), $^6\Sigma/^6A'$ (3.37 eV), and $^4A'$ (4.48 eV) (Table 3).

Re^+-C. Formation of ReC^+ in reaction 3 has a measured threshold of 3.12 ± 0.03 eV (Table 1). From eq 10 and $D_0(CD_2-D_2) + D_0(C-D_2) = 8.20 \pm 0.01$ eV, this threshold yields a BDE for Re^+-C of 5.08 ± 0.03 eV. The value of E_0 for Re^+-C obtained in the CH_4 system is 2.90 ± 0.03 eV. By use of eq 10 and $D_0(CH_2-H_2) + D_0(C-H_2) = 8.06 \pm 0.01$ eV, a BDE for Re^+-C is determined to be 5.16 ± 0.03 eV, in good agreement with the value from the CD_4 system. Our best experimental determination for $D_0(Re^+-C)$ is the weighted average of these two values, 5.12 ± 0.04 eV, where the uncertainty is 2 standard deviations of the mean. As for $ReCH^+$, competition with other channels is probably not an important factor for this process, but the bond energy is most conservatively viewed as a lower limit to the true thermodynamic value.

The experimental value obtained is in reasonable agreement with the results of the present calculations, 4.78 (HW+) and 4.69 (SD) eV (Table 2). Again, the BHLYP functional provides bond energies well below experiment, 3.68 (HW+) and 3.63 (SD) eV, and the QCISD(T) is somewhere between the two density functional methods at 4.48 eV. Clearly, the BHLYP functional provides less accurate predictions for all multiply bound species ($ReCH_2^+$, $ReCH^+$, and ReC^+) compared to the B3LYP functional (MADs of about 1.0 vs 0.20 eV, respectively), whereas the QCISD(T) also performs reasonably well (MAD of 0.31 eV).

The ground state of ReC^+ is calculated to be $^3\Sigma^-$ such that a Re≡C triple bond is formed. The valence electron configuration is $\sigma^2\pi^4\delta^2$, where the orbitals are comparable to those described above for $ReCH^+$. The lowest lying excited state is $^5\Sigma^-$ ($\sigma^1\pi^4\delta^2\sigma^1$) lying 0.71 eV higher in energy. Other excited states include $^5\Pi$ (1.36 eV), $^3\Delta$ (2.15 eV), $^3\Pi$ (4.20 eV), and $^1\Sigma$ (7.08 eV) (Table 3).

Bond-Energy and Bond-Order Correlation for Re^+-CH_x Bonds. One interesting way of investigating the bond order of

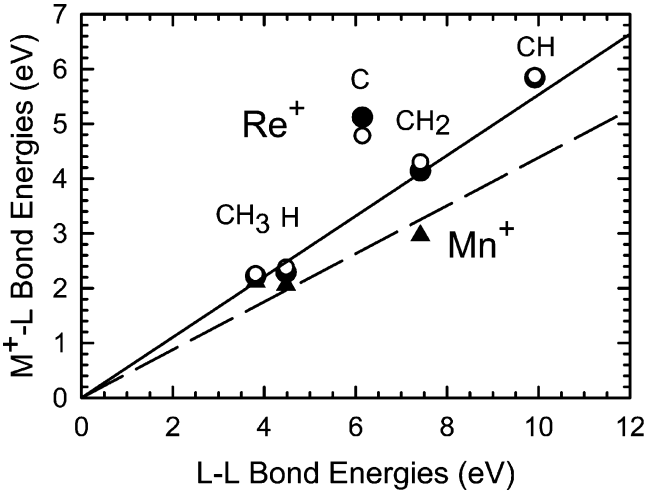

Figure 4. Correlation of Re^+-L bond energies with those for the organic analogues, L−L. Re^+-L values are from Table 2 and include both experiment (closed circles) and theory (open circles, BHLYP/HW+/6-311++G(3df,3p) for ReH^+ and $ReCH_3^+$ and B3LYP/HW+/6-311++G(3df,3p) for all others). The line is a linear regression fit to the experimental data, excluding Re^+-C, constrained to pass through the origin to emphasize the bond-order correlations. Data for MnH^+, $MnCH_3^+$, and $MnCH_2^+$ (taken from refs 59−61) are shown by triangles, and the dashed line is a linear regression fit to these data.

simple metal−ligand species is to compare with organic analogues, i.e., $D_0(Re^+-L)$ versus $D_0(L-L)$. Such a plot is shown in Figure 4. It can be seen that the correlation is remarkably good, which indicates that Re^+-H and Re^+-CH_3 are single bonds, $Re^+=CH_2$ is a double bond, and $Re^+\equiv CH$ is a triple bond. (The linear regression line in Figure 4 is constrained to include the origin to emphasize the bond-order correlation of the ReL^+ vs L_2 species.) The point that lies furthest from the line is for Re^+-C, which is compared with the BDE of C_2. In this case, the Re^+-C BDE is stronger than predicted by this simple correlation because the covalent double bond in this molecule is augmented by back-donation of an occupied 5d orbital on Re^+ into the empty 2p orbital on C. Such an interaction cannot occur in the C_2 molecule. Also illustrated in Figure 4 is the relatively good agreement between experiment and theory: B3LYP/HW+ for multiply bonded species and BHLYP/HW+ for the singly bonded species.

It is also interesting to compare these results to those for the first-row congener, Mn^+. Values for the second-row congener, Tc^+, are not available because of the difficulties of dealing with this radioactive element. Bond energies for MnH^+ and $MnCH_3^+$ are 2.06 ± 0.14[9a,59] and 2.12 ± 0.04 eV,[9a,60,61] respectively, whereas that for $MnCH_2^+$ is 2.96 ± 0.09 eV.[9a,61] Figure 4 shows that the singly bonded manganese species have slightly weaker bonds than ReH^+ and $ReCH_3^+$ (by an average of 0.2 eV), but the double bond to manganese is clearly much weaker than that to rhenium (by 1.2 eV). On average, the linear regression lines indicate that the bonds to Re^+ are 25% greater than those to Mn^+, an effect of the lanthanide contraction.

Potential Energy Surfaces of $[ReCH_4]^+$

The potential energy surfaces for interaction of Re^+ with methane are shown in Figure 5. All energies were calculated at the B3LYP/HW+/6-311+G(3df,3p) level of theory and include zero-point energy corrections (unscaled). In most cases, transition states were located using the synchronous transit-guided quasi-Newton method (QST3)[62,63] followed by geometry optimizations and frequency calculations to verify a first-order saddle point. As suggested above, the B3LYP level of theory

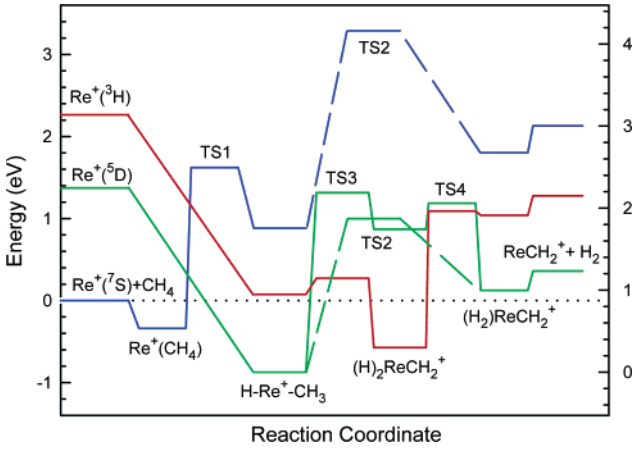

Figure 5. $[ReCH_4]^+$ potential energy surfaces derived from theoretical results. The relative energies of all species are based on ab initio calculations (B3LYP/HW+/6-311++G(3df,3p); see Tables 3 and 5). Energies on the left are relative to the Re^+ (^7S) + CH_4 ground-state asymptote, whereas those on the right are referenced to the $HReCH_3^+$ ($^5A'$) intermediate.

TABLE 5: Theoretical Energies of Intermediates and Transition States Calculated at the B3LYP/HW+/6-311++G(3df,3p) Level of Theory

compd	state	energy (h)	zero-point energy (h)	E_{rel} (eV)[a]
$Re^+(^7S) + CH_4$		−119.209 316	0.044 525	0.000
$Re^+(CH_4)$	$^7A_1$	−119.221 748	0.044 824	−0.330
TS1	$^7A'$	−119.141 074	0.035 975 (1 imag)	1.621
$HReCH_3^+$	$^5A'$	−119.237 135	0.040 256	−0.873
	^3A	−119.202 123	0.040 094	0.075
	$^3A'$	−119.197 640	0.039 995	0.194
	$^3A''$	−119.174 972	0.040 299	0.819
	$^7A_1$	−119.171 916	0.039 523	0.882
TS2	$^5A'$	−119.163 029	0.034 930 (1 imag)	0.998
	$^7A'$	−119.078 532	0.031 568 (1 imag)	3.206
TS3	^3A	−119.191 409	0.036 560 (1 imag)	0.271
	^5A	−119.151 685	0.035 201 (1 imag)	1.315
$(H)_2ReCH_2^+$	^3A	−119.222 479	0.036 611	−0.574
	$^3A''$	−119.220 146	0.035 403 (1 imag)	−0.543
	$^5A_1$	−119.169 545	0.036 706	0.869
	$^3A'$	−119.143 005	0.036 908	1.597
TS4	^3A	−119.159 453	0.034 734 (1 imag)	1.090
	^5A	−119.156 709	0.035 504 (1 imag)	1.186
$(H_2)ReCH_2^+$	$^5B_1$	−119.195 635	0.035 401	0.124
	$^3B_1$	−119.162 198	0.035 461	1.036
	$^7A''$	−119.132 646	0.034 065	1.802
	$^3A_1$	−119.121 483	0.035 217	2.137
	$^5A_1$	−119.089 758	0.036 320	3.030
	$^7A'$	−119.081 984	0.032 491	3.137
$ReCH_2^+ + H_2$	$^5B_1$	−119.183 832	0.032 250	0.359
	$^3B_1$	−119.150 192	0.032 491	1.277
	$^7A'$	−119.118 049	0.031 041	2.117

[a] Energy relative to Re^+ (^7S) + CH_4 reactants including zero-point energies (unscaled).

overbinds species with single covalent bonds to Re^+ but appears to handle multiple bonds adequately. Because nearly all of the species on these surfaces involve several bonds to Re^+, the relative characteristics of the surfaces are likely to be qualitatively correct. Even if the energies are not quantitative, the qualitative characteristics of the surfaces are of the most interest here. Tables 5 and 6 provide summaries of the theoretical results (energies and structures) for each of the intermediates and transition states.

Septet Surface. Interaction of $Re^+(^7S, 6s^15d^5)$ with methane leads initially to the formation of a $Re^+(CH_4)$ adduct in which the methane molecule remains intact and largely unperturbed. The methane binds in an η^3 conformation in a $^7A_1$ state (C_{3v}

TABLE 6: Theoretical Structures of Intermediates and Transition States Calculated at the B3LYP/HW+/6-311++G(3df,3p) Level of Theory[a]

compd	state	r(Re−H)	r(Re−C)	r(C−H)	r(H−H)	∠ReCH	∠HCH	∠HReC	∠HReH	dihedral angle
$ReCH_4^+$	$^7A_1$	2.816 (3)	2.926	1.092		73.4 (3)	106.6 (3)			±120.0
				1.094 (3)		180.0	112.2 (3)			
TS1	$^7A'$	1.650	3.468	1.079		91.9 (2)	119.0 (2)	63.2		0.0
				1.081 (2)		100.5	120.0			±120.0
$HReCH_3^+$	$^5A'$	1.640	2.037	1.093 (2)		106.0	110.2 (2)	104.4		164.1
				1.100		109.8 (2)	110.8			
	^3A	1.632	2.019	1.094		107.2	110.4 (3)	104.8		171.1
				1.096		108.1				
				1.099		110.2				
	$^3A'$	1.633	2.015	1.096 (2)		106.9	109.9	109.2		±60.0
				1.099		109.4 (2)	110.6 (2)			180.0
	$^3A''$	1.630	2.001	1.098 (3)		107.3 (2)	109.9 (2)	99.9		±60.0
						110.2	112.2			180.0
	$^7A_1$	1.691	2.411	1.087 (3)		99.4 (3)	117.4 (3)	180.0		0, ±120.0
TS2	$^5A'$	1.656	1.938	1.091 (2)	1.244	121.9 (2)	107.1 (2)	76.2	43.5	±83.3
		1.702					114.8	119.7		
	$^7A'$	1.642	2.402	1.082 (2)	2.646	110.8 (2)	109.6 (2)	69.7	105.5	±99.3
		1.681					136.7	175.3		
TS3	^3A	1.756	1.880	1.089	2.450	113.5	100.8	109.6	92.8	9.1, 177.8
		1.627		1.099		130.7	113.5			
				1.339			115.5			
	^5A	1.658	2.001	1.092	2.938	119.4	116.6	65.2	124.2	15.7, 105.1,
		1.666		1.087		123.4		122.2		119.6, 124.2
$(H)_2ReCH_2^+$	^3A	1.627	1.835	1.098	2.443	118.7	116.4	89.9	97.0	3.8, 83.7,
		1.635		1.092		124.9		107.1		93.4, 179.1
	$^3A''$	1.628 (2)	1.841	1.094 (2)	2.220	122.1 (2)	115.8	93.2 (2)	86.0	±46.2, ±132.3
	$^5A_1$	1.658 (2)	1.965	1.091 (2)	2.959	121.2	117.5		126.3	±90.0
						121.3				
	$^3A'$	1.625 (2)	1.986	1.094 (2)	2.220	123.1 (2)	113.9	98.7 (2)	106.9	±35.2, ±143.9
TS4	^3A	2.245	1.848	1.092	0.769	121.1	114.8	136.6	19.8	49.0, 78.6,
		2.222		1.095		123.9		140.8		96.3, 125.8
	^5A	1.624	2.015	1.088	1.859	121.0	115.7	83.9	69.3	32.0, 74.3,
		1.646		1.091		121.8		126.1		90.8, 133.0
$(H_2)ReCH_2^+$	$^5B_1$	2.314 (2)	1.878	1.093 (2)	0.761	123.2 (2)	113.5	170.5 (2)	18.9	0.0
	$^3B_1$	2.304 (2)	1.860	1.094 (2)	0.762	123.3 (2)	113.4	170.5 (2)	19.0	0.0
	$^7A''$	2.226 (2)	2.078	1.086 (2)	0.769	121.4 (2)	117.3	170.0 (2)	19.9	90.0
	$^3A_1$	2.423 (2)	1.821	1.096 (2)	0.759	122.6 (2)	114.8	171.0 (2)	18.0	90.0
	$^5A_1$	1.991 (2)	1.949	1.092 (2)	0.817	122.3 (2)	115.5	168.2 (2)	23.7	90.0
	$^7A'$	1.701	2.258	1.085 (2)	1.815	113.7	132.4	120.7	65.9	90.0
		1.637				113.8		173.4		

[a] Bond lengths are in Å. Bond angles are in degrees. Degeneracies are listed in parentheses.

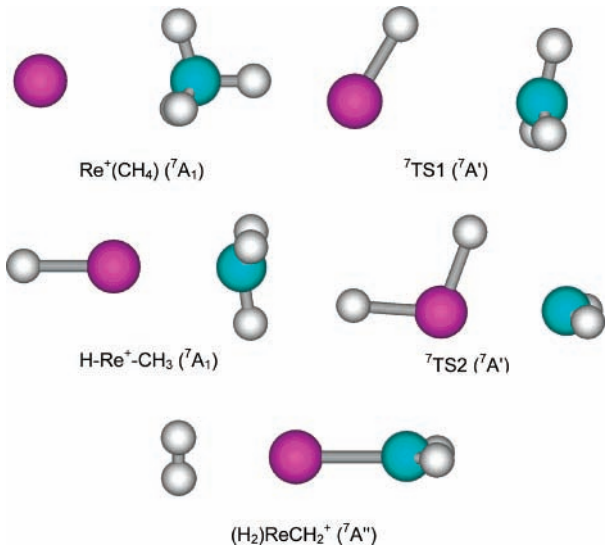

Figure 6. Structures of several intermediates and transition states along the septet surface of the $[ReCH_4]^+$ system calculated at the B3LYP/HW+/6-311++G(3df,3p) level of theory.

symmetry) (Figure 6). Upon further reduction of the Re−H bond distance, the system passes over a transition state, ^{7}TS1, leading to the insertion intermediate $H-Re^+-CH_3$. This transition state has C_s symmetry and an H−Re−C bond angle of 63° (Figure 6). On the septet surface, the $HReCH_3^+$ intermediate retains the $^7A_1$ state and has C_{3v} symmetry and a H−Re−C bond angle of 180° (Figure 6). The Re−H bond distance, 1.69 Å, is comparable to that of $Re-H^+$ ($^6\Sigma^+$), 1.65 Å, but the Re−C bond distance of 2.41 Å is substantially longer than in $ReCH_3^+$ ($^6A_1$), 2.06 Å. This observation along with the Re−C−H bond angles of 99° indicate that the methyl group is loosely bound to the ReH^+ molecule in this state. The HRe^+-CH_3 bond energy is calculated to be 0.90 eV.

Continuing along the septet surface, the system passes over ^{7}TS2, in which an H_2 bond begins to form. This transition state has C_s symmetry and a $^7A'$ state (Figure 6). The Re−C bond distance is quite long (2.40 Å), indicating that the CH_2 group is loosely bound. This leads to formation of a $(H_2)ReCH_2^+$ intermediate, which has a $^7A''$ ground state (a $^7A'$ state lies 1.33 eV higher in energy). In this intermediate, the H_2 bond distance is 0.769 Å compared to that for free H_2, 0.742 Å, and the geometry of the $ReCH_2^+$ part of the molecule is similar to that for $ReCH_2^+$ ($^7A'$), although planar (Figure 6). Overall, this is consistent with the weak $H_2-ReCH_2^+$ bond energy, calculated to be only 0.31 eV.

Quintet Surface. Reaction of methane with Re^+ in its quintet state proceeds directly to formation of the insertion intermediate, $HReCH_3^+$ ($^5A'$), the global minimum of the $[ReCH_4^+]$

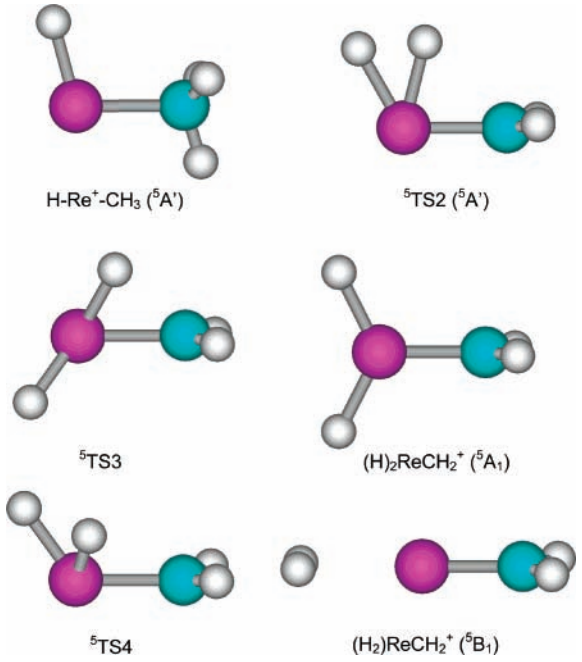

Figure 7. Structures of several intermediates and transition states along the quintet surface of the $[ReCH_4]^+$ system calculated at the B3LYP/HW+/6-311++G(3df,3p) level of theory.

system. Several attempts to locate a $Re^+(CH_4)$ on the quintet surface species always collapsed directly to this intermediate. This observation is consistent with calculations of Dai and Balasubramanian on the related $Re^+ + H_2$ system,[54] where both the quintet and triplet states of Re^+ insert spontaneously into H_2 to form the rhenium dihydride cation. This intermediate has a HReC bond angle of 104° (Figure 7), with Re−H and Re−C bond distances (1.64 and 2.04 Å) comparable to those of ReH^+ ($^6\Sigma^+$) and $ReCH_3^+$ ($^6A_1$) (1.65 and 2.06 Å). This indicates that two covalent single bonds are formed using sd hybrids on the rhenium cation, leaving the four π and δ-like nonbonding orbitals on the metal ion singly occupied.

From $HReCH_3^+$ ($^5A'$), the system can again proceed directly to a $(H_2)ReCH_2^+$ intermediate via the four-centered transition state ^{5}TS2 having A′ symmetry (Figure 7). In this species, the Re−H (1.66 and 1.70 Å) bond distances are comparable to those of isolated ReH^+ ($^6\Sigma^+$), 1.65 Å, whereas the Re−C (1.94 Å) bond distance falls between those of $ReCH_2^+$ ($^5B_1$), 1.86 Å, and $ReCH_3^+$ ($^6A_1$), 2.06 Å. This transition state lies 1.87 eV above $HReCH_3^+$ ($^5A'$) and 1.0 eV above the ground-state reactants. The $(H_2)ReCH_2^+$ intermediate has a $^5B_1$ ground state with a $^5A_1$ state lying 2.91 eV higher in energy. The $^5B_1$ state lies 0.24 eV below the $ReCH_2^+$ ($^5B_1$) + H_2 ($^1\Sigma_g^+$) asymptote, the overall ground state of this product channel. This weak bond is consistent with the H_2 bond length of 0.761 Å compared to that of free H_2, 0.742 Å, and similar $ReCH_2^+$ units (Figure 7).

An alternative pathway for transformation between the $HReCH_3^+$ and $(H_2)ReCH_2^+$ intermediates was also located. This involves sequential α-H migrations through a dihydride intermediate, $(H)_2ReCH_2^+$, which lies 0.87 eV above the ground-state reactants and 1.74 eV above the $HReCH_3^+$ intermediate. The dihydride has a $^5A_1$ state with C_{2v} symmetry in which the planes defined by HReH and $ReCH_2$ are perpendicular (Figure 7). Re−H (1.66 Å) and Re−C (1.96 Å) bond distances indicate covalent bonding interactions. From $HReCH_3^+$, the dihydride is reached via ^{5}TS3 (Figure 7), lying 0.45 eV higher in energy than $(H)_2ReCH_2^+$ ($^5A_1$), and is the rate-limiting step for this pathway at 1.32 eV above the ground-state reactants. The dihydride converts to the $(H_2)ReCH_2^+$ intermediate through

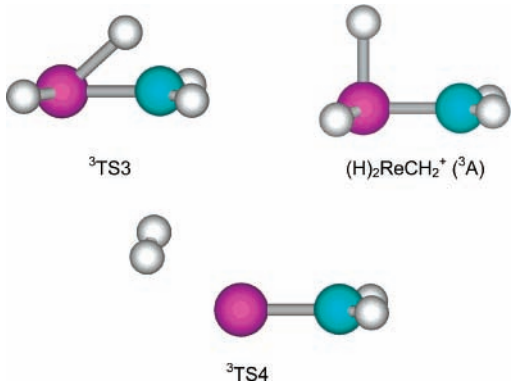

Figure 8. Structures of several intermediates and transition states along the triplet surface of the $[ReCH_4]^+$ system calculated at the B3LYP/HW+/6-311++G(3df,3p) level of theory. Triplet state structures for $H-Re^+-CH_3$ and $(H_2)ReCH_2^+$ appear nearly identical to those shown for the quintet analogues in Figure 7.

^{5}TS4 (Figure 7), which lies 0.32 eV above the dihydride. Overall, it can be seen that the transition states for the sequential α-H migration pathway are slightly higher in energy than the four-centered pathway of ^{5}TS2 (Figure 5).

Triplet Surface. The triplet state of Re^+ is also calculated to spontaneously insert into the C−H bond of methane without forming a $Re^+(CH_4)$ intermediate. The triplet $HReCH_3^+$ species lies above the comparable species having quintet spin, as would be expected according to Hund's rules for a species forming two covalent bonds and having four nonbonding orbitals. This triplet intermediate has a structure similar to that shown for the quintet spin analogue in Figure 7. It nearly has C_s symmetry but the most stable geometry (∠HReC = 105° and ∠HReCH = 171°) was calculated to lie 0.12 eV lower in energy than a $^3A'$ state (and a $^3A''$ state was found with an excitation energy of 0.74 eV). No four-centered transition state (^{3}TS2) could be found on the triplet surface, but formation of ^{3}TS3 (Figure 8) involves only a small barrier of 0.20 eV. This leads to the lowest energy form of the dihydride, $(H)_2ReCH_2^+$, a ^3A state (Figure 8), the spin state anticipated for a molecule with four covalent bonds to Re^+ and two nonbonding orbitals. Note that the two Re−H (1.63 and 1.64 Å) and Re−C (1.84 Å) bonds are nearly perpendicular to each other with bond lengths nearly identical to those of ReH^+ ($^6\Sigma^+$) (1.65 Å) and $ReCH_2^+$ ($^5B_1$) (1.86 Å). A low-lying $^3A''$ state (0.03 eV above the ground state) was found with an imaginary frequency (-221 cm^{-1}) corresponding largely to a rotation about the Re−C bond axis until the two ReH bonds are symmetrically oriented on either side of the Re−C π bond. A $^3A'$ state was also located 2.17 eV above the lowest energy state.

The triplet dihydride intermediate begins to eliminate dihydrogen by passing over ^{3}TS4, which lies 1.66 eV higher in energy but only 0.05_5 eV above the lowest triplet state of $(H_2)ReCH_2^+$ ($^3B_1$). Figure 8 shows that this transition state has a geometry similar to that of the $(H_2)ReCH_2^+$ intermediate, which looks essentially the same as the quintet analogue (Figure 7). This latter intermediate is planar and has C_{2v} symmetry and an H_2 bond distance of 0.762 Å compared to free H_2 at 0.742 Å. Loss of dihydrogen to form $ReCH_2^+$ ($^3B_1$) requires only 0.24 eV. A $(H_2)ReCH_2^+$ complex in a $^3A_1$ state was also found lying 1.10 eV above the $^3B_1$ state.

Re^+-CH_4 Bond Energy. Collision-induced dissociation of the $ReCH_4^+$ species leads predominantly to formation of $Re^+ + CH_4$ (reaction 7) with a threshold of 0.53 ± 0.15 eV. Of the various intermediates identified on the global $[ReCH_4^+]$ potential energy surfaces, only $Re^+(CH_4)$ ($^7A_1$), $HReCH_3^+$ ($^5A'$), and

$(H)_2ReCH_2^+$ (^3A) lie below the energy of the Re^+ (^7S) + CH_4 asymptote (Figure 5). (B3LYP/HW+ values are used in the discussion here, whereas values for alternative levels of theory are given in Table 2. As found above, this level of theory appears to provide the most reasonable values for species with multiple bonds to Re^+. For the noncovalent $Re^+(CH_4)$ ($^7A_1$) species, all levels of theory provide about the same energetics.) Given the accuracy of the theoretical bond energies discussed above, the calculated well-depths for $Re^+(CH_4)$ ($^7A_1$), 0.33 eV, $HReCH_3^+$ ($^5A'$), 0.87 eV, and $(H)_2ReCH_2^+$ (^3A), 0.57 eV, are all consistent with the experimental value of 0.53 ± 0.15 eV. If the molecule experimentally characterized were either of the latter two species, then it seems likely that CID would also form ReH^+ at lower energies and more efficiently than is observed here (as for instance was observed for CID of $HPtCH_3^+$).[7] Thus, it seems likely that the process observed experimentally corresponds to dissociation of $Re^+(CH_4)$ ($^7A_1$), consistent with formation of this molecule by collisional stabilization of Re^+ (^7S) interacting with CH_4. The observation that $ReCH_2^+$ and ReH^+ are not formed until much higher energies seems consistent with a complex in which the CH bonds have not been activated. Further, this suggests that the crossing point between the septet and quintet surfaces may lie above the Re^+ (^7S) + CH_4 asymptote; otherwise, formation of $HReCH_3^+$ ($^5A'$) in the flow tube would seem more probable and CH bond activation steps upon collisional activation might be more competitive with loss of the intact ligand.

Discussion

For reaction of Re^+ (^7S) with methane, the dehydrogenation reaction is endothermic. Reasonable agreement between theoretical and experimental bond energies indicates that the $ReCH_2^+$ product is formed in its $^5B_1$ ground state at threshold. This process must occur without activation energy in excess of the endothermicity because Irikura and Beauchamp observed that the reverse of reaction 5 occurs at thermal energies.[2] Further, there is strong competition evident between the formation of $ReCH_2^+ + H_2$ and $ReH^+ + CH_3$, implying a common intermediate. To estimate the absolute efficiency of the dehydrogenation reaction, we performed phase space theory calculations using molecular parameters (vibrational and rotational constants) calculated here. In these calculations, the absolute magnitude of the cross section is set by the LGS collision limit.[31] Hence, the only adjustable parameter in the phase space calculation is the endothermicity for reaction 5, $E_0(5)$. The results of this calculation for $E_0(5) = 0.60$ eV, slightly below the final threshold suggested by our best value for $D_0(Re^+-CH_2)$ (Table 2), are shown in Figure 1. This value was chosen because it reproduces the threshold region accurately. It can be seen that the phase space prediction reproduces this data set both in magnitude and energy dependence for an extended range. On average, the experimental data lie 14 ± 10% below the phase space prediction, indicating that the reaction occurs on 86% of all collisions. Calculations were also performed including or excluding the competition with reaction 2, with a threshold set to the optimum value calculated from the bond energies in Table 2. Figure 1 shows that the decline in the $ReCD_2^+$ cross section is nicely reproduced when this competition is included. Further, the competitive shift hypothesized above for the ReD^+ cross section is observed in this calculation.

σ-Bond activation by atomic metal ions can be understood using a simple donor−acceptor model. Such reactions require electronic configurations in which there is an empty acceptor orbital on the metal ion into which the electrons of a bond to be broken are donated. Concomitantly, metal electrons in orbitals having π-symmetry back-donate into the antibonding orbital of the bond to be broken. If the acceptor orbital is occupied, a repulsive interaction can result leading to inefficient reaction either by more direct abstraction pathways or by introduction of a barrier to the reaction. In our previous studies, the activation of methane by atomic metal ions was explained by this simple donor−acceptor model, which leads to an oxidative addition mechanism.[9] In such a mechanism,[55−57,64−68] oxidative addition of a C−H bond to M^+ forms a $H-M^+-CH_3$ intermediate. Products can be formed by the reductive elimination of H_2 at low energies by metal−hydrogen or metal−carbon bond cleavage at high energies and by further dehydrogenation of primary products at still higher energies. For first-row transition metal ions,[9] the reductive elimination process proceeds through a four-centered transition state from the $H-M^+-CH_3$ intermediate to a $(H_2)MCH_2^+$ intermediate in which a hydrogen molecule is electrostatically bound to the MCH_2^+ species. This latter intermediate then decomposes by expulsion of H_2. The calculated potential energy surface for the reaction of Re^+ with methane (Figure 5) illustrates all of these features and allows a detailed interpretation of the mechanism for this reaction system.

Mechanism for Dehydrogenation of Re^+ with Methane. On the septet surface, both ^{7}TS1 and ^{7}TS2 are much higher in energy than the $ReCH_2^+$ product formed in an endothermic process with a threshold of only 0.6 eV (Table 1). Because Re^+ (^7S, $6s^15d^5$) has no empty valence orbitals, the simple donor−acceptor process is restricted, leading to the high barrier for ^{7}TS1. The energy of ^{7}TS2 is even higher because the high spin does not allow formation of the several covalent bonds needed to stabilize this transition state. Thus, at low energies, reaction of Re^+ (^7S) with methane must occur by coupling to the quintet surface where oxidative addition of CH_4 to Re^+ produces a $^5A'$ hydridomethylrhenium cation intermediate, $H-Re^+-CH_3$, the global minimum on the potential energy surface (Figure 5). On the quintet surface, the empty s orbital on Re^+ (^5D, $5d^6$) acts as an efficient acceptor orbital, and a doubly occupied $5d\pi$ orbital can provide an efficient donor orbital. This leads naturally to an intermediate in which the Re^+ forms two bonds using 6s5d hybrids.

From $H-Re^+-CH_3$ ($^5A'$), there are two pathways for producing the $(H_2)ReCH_2^+$ ($^5B_1$) intermediate that easily loses dihydrogen to form the ground-state $ReCH_2^+$ ($^5B_1$) + H_2 products. As for the first-row transition metal ions, a four-centered transition state, ^{5}TS2, leads directly between these two intermediates. As found for the dehydrogenation reaction of methane with Pt^+ (^2D),[7,13−15] the activation of a second C−H bond (α-H transfer) can lead to formation of a dihydridomethylenerhenium cation intermediate, $(H)_2ReCH_2^+$ ($^5A_1$). Reductive elimination of dihydrogen then forms the $(H_2)Re^+(CH_2)$ intermediate, an electrostatic complex. The energetics of these two pathways are similar, with rate-limiting transition states of ^{5}TS2 at 1.00 eV and ^{5}TS3 at 1.32 eV. However, both of these pathways are calculated to exceed the energy of the ground-state product asymptote, suggesting that another pathway must be available.

The only pathway available for dehydrogenation that may not involve a barrier must also couple the quintet and triplet surfaces. Once the $H-Re^+-CH_3$ ($^5A'$) intermediate is formed, it can cross over to the triplet state forming the $(H)_2ReCH_2^+$ (^3A) intermediate. The triplet spin state is the lowest energy state for the dihydridomethylenerhenium cation because four covalent bonds to Re^+ are formed to yield the most stable species, leaving only two unpaired electrons. From this inter-

mediate, we imagine that there is a transition state that parallels ^{5}TS4 on the triplet surface, allowing a low-energy pathway for dehydrogenation. This transition state cannot be located using the methodology employed in this study because of the different spin states of the starting, $(H)_2ReCH_2^+$ (^{3}A), and end points, $(H_2)ReCH_2^+$ ($^5B_1$), for this transformation. However, using the geometry of ^{5}TS4, we calculate that a triplet state analogue lies 0.64 eV lower in energy, only 0.55 eV above the ground-state reactants and still below the experimental endothermicity for the dehydrogenation reaction. It is reasonable that this species is lower in energy on the triplet surface because of the similarity between the structures of ^{5}TS4 (Figure 7) and $(H)_2ReCH_2^+$ (^{3}A) (Figure 8).

Finally, we note that the exothermic reactivity observed for unquenched Re^+ ions (Figure 1) can be explained by the presence of small amounts of any excited state of Re^+. Even the first excited state has an excitation energy (1.827 eV)[38] well in excess of the endothermicity of reaction 5. However, excited states above 2.4 eV do not appear to be populated because these could react exothermically to form $ReH^+ + CH_3$, which is not observed. On the basis of the calculated potential energy surfaces, the excited states present should be able to access the adiabatic ground-state surface for dehydrogenation and to pass over all transition states calculated on the quintet and triplet surfaces.

Mechanism for Higher Energy Products. As the energy available increases above about 2 eV, Re^+-H and Re^+-CH_3 products are formed by simple bond cleavages of the $H-Re^+-CH_3$ intermediate. These processes, in particular formation of $ReH^+ + CH_3$, deplete the population of this intermediate such that the cross section for the dehydrogenation process declines commensurately. Because formation of $ReCH_2^+ + H_2$ is thermodynamically preferred by about 1.6 eV (Table 2), this competition indicates that formation of $ReH^+ + CH_3$ must be preferred kinetically. This is consistent with a simple bond cleavage of HRe^+-CH_3 at elevated kinetic energies, whereas the elimination of H_2 occurs via the more restricted pathway discussed above.

In the reaction of Re^+ with CH_4 (CD_4), the ReH^+ (ReD^+) cross section is dominant at energies above 2.5 eV (Figure 1). This is a typical behavior for the reaction of bare metal ions with hydrogen-containing polyatomic molecules.[4,9,55,69] The observation that the $ReH^+ + CH_3$ ($ReD^+ + CD_3$) channel dominates the nearly isoenergetic $ReCH_3^+ + H$ ($ReCD_3^+ + D$) channel (Table 1) is largely a result of angular momentum constraints.[4,55−57] Briefly, because the $ReCH_3^+ + H$ ($ReCD_3^+ + D$) channel has a reduced mass of 1.0 (2.0) amu, much smaller than that of the reactants, 14.7 (18.1) amu, it can only be formed by the reactants that come together with smaller orbital angular momenta, i.e., at small impact parameters. In contrast, the $ReH^+ + CH_3$ ($ReD^+ + CD_3$) channel has a reduced mass of 13.9 (16.4) amu, close to that of the reactants, such that most impact parameters leading to strong interactions between the Re^+ and methane can form these products and still conserve angular momentum. We further note that the branching ratio of $\sigma(ReD^+)/\sigma(ReCD_3^+)$ is about 70 from threshold to about 5 eV, larger than the range of 4−20 suggested as appropriate for a statistical mechanism.[4,45] However, statistical phase space calculations predict an even smaller cross section for $ReCH_3^+$. These comparisons are complicated by the likelihood that $ReCH_3^+$ decomposes to form $ReCH^+$, thereby limiting the magnitude of its cross section.

At high energies, ReC^+ and $ReCH^+$ are formed by dehydrogenation of the primary products, $ReCH_2^+$ and $ReCH_3^+$, respectively. The thermochemistry determined above (Table 2) shows that these dehydrogenations require 2.37 ± 0.08 and 0.99 ± 0.14 eV, respectively. In addition, H atom loss from $ReCH_3^+$, which requires 2.81 ± 0.15 eV, leads to the second feature in the $ReCH_2^+$ cross section (Figure 2). This process is observed because the simple bond cleavage is kinetically more favorable at high energies than the more complex dehydrogenation processes. Comparable observations have been made for second-row metal systems[57,68−71] and for Pt^+.[7]

Conclusions

Ground-state Re^+ ions are found to be reactive with methane over a wide range of kinetic energies. At low energies, dehydrogenation is endothermic but efficient and dominates the product spectrum. At high energies, the dominant process is formation of $ReH^+ + CH_3$, which occurs mainly by simple bond cleavage of a $H-Re^+-CH_3$ intermediate. This channel is favored over the $ReCH_3^+ + H$ channel because of angular momentum constraints. At higher energies, the $ReCH_2^+$ and $ReCH_3^+$ products decompose by dehydrogenation (to form ReC^+ and $ReCH^+$, respectively) and at still higher energies by H atom loss to yield $ReCH^+$ and $ReCH_2^+$.

Analysis of the kinetic energy dependence of the reaction cross sections provides the BDEs of Re^+-CH_3, Re^+-CH_2, Re^+-CH, and Re^+-C. Our experimental results for $D_0(Re^+-CH_3)$ and $D_0(Re^+-H)$ are slightly greater than their manganese analogues;[9a] however, the value for $D_0(Re^+-CH_2)$ is significantly higher than its manganese counterpart. Our experimental BDEs are found to be in good agreement with a variety of ab initio calculations from the literature and performed here (Table 2). Whereas the B3LYP functional performs well for multiply bonded species (ReC^+, $ReCH^+$, and $ReCH_2^+$), as previously observed by Holthausen et al.,[52] the BHLYP functional is needed to reproduce bond energies for ReH^+ and $ReCH_3^+$, as previously concluded by Holthausen et al.[21]

Calculations are also used to provide a detailed potential energy surface for the $ReCH_4^+$ system. This potential energy surface shows that the reaction of Re^+ (^{7}S) with methane proceeds via the oxidative addition of one C−H bond to yield a hydridomethylrhenium intermediate, $H-Re^+-CH_3$ (^{5}A′), the global minimum. $ReH^+ + CH_3$ and $ReCH_3^+ + H$ can be formed by simple bond cleavages from this intermediate. At threshold, $ReCH_2^+ + H_2$ formation appears to involve α-H migration to form the dihydridomethylenerhenium cation, $(H)_2ReCH_2^+$ (^{3}A), followed by reductive elimination of dihydrogen to yield $ReCH_2^+$ ($^5B_1$) + H_2. Overall, dehydrogenation of methane by Re^+ appears to require three spin changes along the lowest energy path available: Re^+ (^{7}S) + CH_4 ($^1A_1$) → $H-Re^+-CH_3$ (^{5}A′) → $(H)_2ReCH_2^+$ (^{3}A) → $(H_2)ReCH_2^+$ ($^5B_1$) → $ReCH_2^+$ ($^5B_1$) + H_2 ($^1\Sigma_g^+$). Despite this requirement, the reaction is found to occur with high efficiency, suggesting that spin conservation is not an impediment for reaction of this heavy metal system.

Acknowledgment. This work is supported by the National Science Foundation, Grant CHE-0135517.

References and Notes

(1) Irikura, K. K.; Beauchamp, J. L. *J. Am. Chem. Soc.* **1991**, *113*, 2769.
(2) Irikura, K. K.; Beauchamp, J. L. *J. Phys. Chem.* **1991**, *95*, 8344.
(3) Ohanessian, G.; Brusich, M. J.; Goddard, W. A., III. *J. Am. Chem. Soc.* **1990**, *112*, 7182.
(4) Sunderlin, L. S.; Armentrout, P. B. *J. Am. Chem. Soc.* **1989**, *111*, 3845.
(5) Chowdhury, A. K.; Wilkins, C. L. *J. Am. Chem. Soc.* **1987**, *109*, 5336.

(6) Irikura, K. K.; Goddard, W. A., III. *J. Am. Chem. Soc.* **1994**, *116*, 8733.
(7) Zhang, X.-G.; Liyanage, R.; Armentrout, P. B. *J. Am. Chem. Soc.* **2001**, *123*, 5563.
(8) Allison, J. *Prog. Inorg. Chem.* **1986**, *34*, 627. Squires, R. R. *Chem. Rev.* **1987**, *87*, 623. *Gas-Phase Inorganic Chemistry*; Russell, D. H., Ed.; Plenum: New York, 1989. Eller, K.; Schwarz, H. *Chem. Rev.* **1991**, *91*, 1121
(9) For recent reviews, see the following. (a) Armentrout, P. B.; Kickel, B. L. In *Organometallic Ion Chemistry*; Freiser, B. S., Ed.; Kluwer: Dordrecht, The Netherlands, 1996; p 1. (b) Armentrout, P. B. In *Topics in Organometallic Chemistry*; Brown, J. M., Hofmann, P., Eds.; Springer-Verlag: Berlin, 1999; Vol. 4-I, p 1.
(10) Crabtree, R. H. *The Organometallic Chemistry of the Transition Metals*, 2nd ed.; Wiley: New York, 1994
(11) Somorjai, G. A. *Introduction to Surface Chemistry and Catalysis*; Wiley: New York, 1994.
(12) Wesendrup, R.; Schröder, D.; Schwarz, H. *Angew. Chem., Int. Ed. Engl.* **1994**, *33*, 1174.
(13) Heinemann, C.; Wesendrup, R.; Schwarz, H. *Chem. Phys. Lett.* **1995**, *239*, 75.
(14) Pavlov, M.; Blomburg, M. R. A.; Siegbahn, P. E. M.; Wesendrup, R.; Heinemann, C.; Schwarz, H. *J. Phys. Chem. A* **1997**, *101*, 1567.
(15) Achatz, U.; Beyer, M.; Joos, S.; Fox, B. S.; Nieder-Schatteburg, G.; Bondybey, V. E. *J. Phys. Chem. A* **1999**, *103*, 8200.
(16) Achatz, U.; Berg, C.; Joos, S.; Fox, B. S.; Beyer, M. K.; Nieder-Schatteburg, G.; Bondybey, V. E. *Chem. Phys. Lett.* **2000**, *320*, 53.
(17) Buckner, S. W.; MacMahon, T. J.; Byrd, G. D. B. S. *Inorg. Chem.* **1989**, *28*, 3511.
(18) Ranasinghe, Y. A.; MacMahon, T. J.; Freiser, B. S. *J. Phys. Chem.* **1991**, *95*, 7721.
(19) Heinemann, C.; Koch, W.; Schwarz, H. *Chem. Phys. Lett.* **1995**, *245*, 509.
(20) Heinemann, C.; Hertwig, R. H.; Wesendrup, R.; Koch, W.; Schwarz, H. *J. Am. Chem. Soc.* **1995**, *117*, 495.
(21) Holthausen, M. C.; Heinemann, C.; Cornehl, H. H.; Koch, W.; Schwarz, H. *J. Chem. Phys.* **1995**, *102*, 4931.
(22) Heinemann, C.; Schwarz, H.; Koch, W.; Dyall, K. G. *J. Chem. Phys.* **1996**, *104*, 4642.
(23) Musaev, D. G.; Morokuma, K. *Isr. J. Chem.* **1993**, *33*, 307.
(24) Perry, J. K.; Ohanessian, G.; Goddard, W. A., III. *Organometallics* **1994**, *13*, 1870.
(25) Loh, S. K.; Hales, D. A.; Lian, L.; Armentrout, P. B. *J. Chem. Phys.* **1989**, *90*, 5466.
(26) Schultz, R. H.; Armentrout, P. B. *Int. J. Mass Spectrom. Ion Processes* **1991**, *107*, 29.
(27) Teloy, E.; Gerlich, D. *Chem. Phys.* **1974**, *4*, 417.
(28) Gerlich, D. *Adv. Chem. Phys.* **1992**, *82*, 1.
(29) Ervin, K. M.; Armentrout, P. B. *J. Chem. Phys.* **1985**, *83*, 166.
(30) Chantry, P. J. *J. Chem. Phys.* **1971**, *55*, 2746.
(31) Gioumousis, G.; Stevenson, D. P. *J. Chem. Phys.* **1958**, *29*, 294.
(32) Kickel, B. L.; Armentrout, P. B. *J. Am. Chem. Soc.* **1995**, *117*, 4057.
(33) Clemmer, D. E.; Chen, Y.-M.; Khan, F. A.; Armentrout, P. B. *J. Phys. Chem.* **1994**, *98*, 6522.
(34) Haynes, C. L.; Armentrout, P. B. *Organometallics* **1994**, *13*, 3480.
(35) Kickel, B. L.; Armentrout, P. B. *J. Am. Chem. Soc.* **1995**, *117*, 764.
(36) Chen, Y.-M.; Elkind, J. L.; Armentrout, P. B. *J. Phys. Chem.* **1995**, *99*, 10438.
(37) Sievers, M. R.; Chen, Y.-M.; Armentrout, P. B. *J. Phys. Chem.* **1996**, *100*, 54.
(38) Moore, C. E. *Atomic Energy Levels*; NSRDS-NBS35: Washington, DC, 1971; Vol. III, p 1.
(39) Dalleska, N. F.; Honma, K.; Sunderlin, L. S.; Armentrout, P. B. *J. Am. Chem. Soc.* **1994**, *116*, 3519.
(40) Schultz, R. H.; Armentrout, P. B. *J. Chem. Phys.* **1992**, *96*, 1046.
(41) Schultz, R. H.; Crellin, K. C.; Armentrout, P. B. *J. Am. Chem. Soc.* **1991**, *113*, 8590.
(42) Khan, F. A.; Clemmer, D. C.; Schultz, R. H.; Armentrout, P. B. *J. Phys. Chem.* **1993**, *97*, 7978.
(43) Rodgers, M. T.; Armentrout, P. B. *J. Phys. Chem. A* **1997**, *101*, 1238.
(44) Chesnavich, W. J.; Bowers, M. T. *J. Phys. Chem.* **1979**, *83*, 900.
(45) Aristov, N.; Armentrout, P. B. *J. Am. Chem. Soc.* **1986**, *108*, 1806.
(46) Armentrout, P. B. In *Advances in Gas-Phase Ion Chemistry*; Adams, N. G., Babcock, L. M., Eds.; JAI: Greenwich, CT, 1992; Vol. 1, p 83.
(47) Shimanouchi, T. *Tables of Molecular Vibrational Frequencies*; NSRDS-NBS39: Washington, DC, 1972; Consolidated Vol. I, p 1.
(48) Becke, A. D. *J. Chem. Phys.* **1993**, *98*, 5648.
(49) Lee, C.; Yang, W.; Parr, R. G. *Phys. Rev. B* **1988**, *37*, 785.
(50) Frisch, M. J.; Trucks, G. W.; Schlegel, H. B.; Scuseria, G. E.; Robb, M. A.; Cheeseman, J. R.; Zakrzewski, V. G.; Montgomery, J. A., Jr.; Stratmann, R. E.; Burant, J. C.; Dapprich, S.; Millam, J. M.; Daniels, A. D.; Kudin, K. N.; Strain, M. C.; Farkas, O.; Tomasi, J.; Barone, V.; Cossi, M.; Cammi, R.; Mennucci, B.; Pomelli, C.; Adamo, C.; Clifford, S.; Ochterski, J.; Petersson, G. A.; Ayala, P. Y.; Cui, Q.; Morokuma, K.; Salvadore, P.; Dannenburg, J. J.; Malick, D. K.; Rabuck, A. D.; Raghavachari, K.; Foresman, J. B.; Cioslowski, J.; Ortiz, J. V.; Stefanov, B. B.; Liu, G.; Liashenko, A.; Piskorz, P.; Komaromi, I.; Gomperts, R.; Martin, R. L.; Fox, D. J.; Keith, T.; Al-Laham, M. A.; Peng, C. Y.; Nanayakkara, A.; Gonzalez, C.; Challacombe, M.; Gill, P. M. W.; Johnson, B. G.; Chen, W.; Wong, M. W.; Andres, J. L.; Head-Gordon, M.; Replogle, E. S.; Pople, J. A. *Gaussian 98*, revision A.11; Gaussian, Inc.: Pittsburgh, PA, 2001.
(51) Hay, P. J.; Wadt, W. R. *J. Chem. Phys.* **1985**, *82*, 299.
(52) Holthausen, M. C.; Mohr, M.; Koch, W. *Chem. Phys. Lett.* **1995**, *240*, 245.
(53) Andrae, D.; Haeussermann, U.; Dolg, M.; Stoll, H.; Preuss, H. *Theor. Chim. Acta* **1990**, *77*, 123.
(54) Dai, D.; Balasubramanian, K. *J. Chem. Phys.* **1991**, *95*, 4284.
(55) Aristov, N.; Armentrout, P. B. *J. Phys. Chem.* **1987**, *91*, 6178.
(56) Sunderlin, L. S.; Armentrout, P. B. *J. Phys. Chem.* **1988**, *92*, 1209.
(57) Chen, Y.-M.; Armentrout, P. B. *J. Phys. Chem.* **1995**, *99*, 10775.
(58) Armentrout, P. B.; Li, F.-X. *J. Chem. Phys.* **2004**, *121*, 248.
(59) Elkind, J. L.; Armentrout, P. B. *J. Chem. Phys.* **1986**, *84*, 4862.
(60) Georgiadis, R.; Armentrout, P. B. *Int. J. Mass Spectrom. Ion Processes* **1989**, *91*, 123.
(61) Sunderlin, L. S.; Armentrout, P. B. *J. Phys. Chem.* **1990**, *94*, 3589.
(62) Peng, C.; Schlegel, H. B. *Isr. J. Chem.* **1994**, *33*, 449.
(63) Peng, C.; Ayala, P. Y.; Schlegel, H. B.; Frisch, M. J. *J. Comput. Chem.* **1996**, *17*, 49.
(64) Schultz, R. H.; Elkind, J. L.; Armentrout, P. B. *J. Am. Chem. Soc.* **1988**, *110*, 411.
(65) Georgiadis, R.; Armentrout, P. B. *J. Phys. Chem.* **1988**, *92*, 7067.
(66) Haynes, C. L.; Chen, Y.-M.; Armentrout, P. B. *J. Phys. Chem.* **1995**, *99*, 9110.
(67) Haynes, C. L.; Chen, Y.-M.; Armentrout, P. B. *J. Phys. Chem.* **1996**, *100*, 111.
(68) Sievers, M. R.; Chen, Y.-M.; Haynes, C. L.; Armentrout, P. B. *Int. J. Mass Spectrom. Ion Processes* **2000**, *195/196*, 149.
(69) Chen, Y.-M.; Sievers, M. R.; Armentrout, P. B. *Int. J. Mass Spectrom. Ion Processes* **1997**, *167/168*, 195.
(70) Chen, Y.-M.; Armentrout, P. B. *J. Am. Chem. Soc.* **1995**, *117*, 9291.
(71) Armentrout, P. B.; Chen, Y.-M. *J. Am. Soc. Mass Spectrom.* **1999**, *10*, 821.